

On the Compositional Generalization of Multimodal LLMs for Medical Imaging

Zhenyang Cai[†], Junying Chen[†], Rongsheng Wang[†], Weihong Wang,
Yonglin Deng, Dingjie Song, Yize Chen, Zixu Zhang, Benyou Wang*

The Chinese University of Hong Kong, Shenzhen
wangbenyou@cuhk.edu.cn

Abstract

Multimodal large language models (MLLMs) hold significant potential in the medical field, but their capabilities are often limited by insufficient data in certain medical domains, highlighting the need for understanding what kinds of images can be used by MLLMs for generalization. Current research suggests that multi-task training outperforms single-task as different tasks can benefit each other, but they often overlook the internal relationships within these tasks, providing limited guidance on selecting datasets to enhance specific tasks. To analyze this phenomenon, we attempted to employ *compositional generalization* (CG)—the ability of models to understand novel combinations by recombining learned elements—as a guiding framework. Since medical images can be precisely defined by **Modality**, **Anatomical area**, and **Task**, naturally providing an environment for exploring CG. Therefore, we assembled 106 medical datasets to create **Med-MAT** for comprehensive experiments. The experiments confirmed that MLLMs can use CG to understand unseen medical images and identified CG as one of the main drivers of the generalization observed in multi-task training. Additionally, further studies demonstrated that CG effectively supports datasets with limited data and delivers consistent performance across different backbones, highlighting its versatility and broad applicability. Med-MAT is publicly available at github.com/FreedomIntelligence/Med-MAT.

1 Introduction

Multimodal large language models (MLLMs) (Liu et al., 2023; Li et al., 2024; Chen et al., 2024b) are showing great promise for the medical community, facilitating efficient consultations for doctors and providing patients with anytime access to their medical conditions. However, limited data on rare or privacy-restricted diseases often restricts

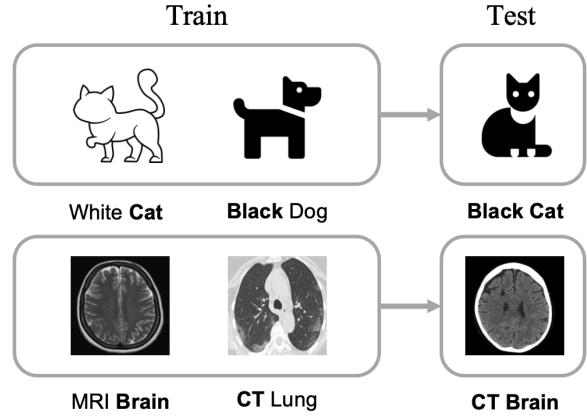


Figure 1: Examples of *Compositional Generalization*: The model is required to understand unseen images by recombining the fundamental elements it has learned.

MLLMs’ performance, making it crucial to explore what kinds of images can be used by MLLMs to generalize these diseases or learn them efficiently.

Current research on medical image generalization (Mo and Liang, 2024; Ren et al., 2024) has demonstrated that models trained on multiple tasks outperform those trained on a single task as they can leverage potential knowledge from other tasks. However, these studies have not conducted a detailed analysis of which data within multitask datasets can mutually complement each other. Consequently, we aim to investigate the phenomenon of mutual improvement in MLLMs’ understanding of medical images from the perspective of composition generalization.

Compositional generalization (CG) (Xu et al., 2022; Li et al., 2019) refers to a model’s ability to learn fundamental elements and recombine them in novel ways to understand unseen combinations (Figure 1). In medical imaging, each image can be categorized by **Modality**, **Anatomical area**, and **medical Task**, presenting numerous natural opportunities for CG. We defined these three elements as the **MAT-Triplet** and collected 106 medical datasets, subsequently merging those that share the

[†]Corresponding author. *Equal Contribution.

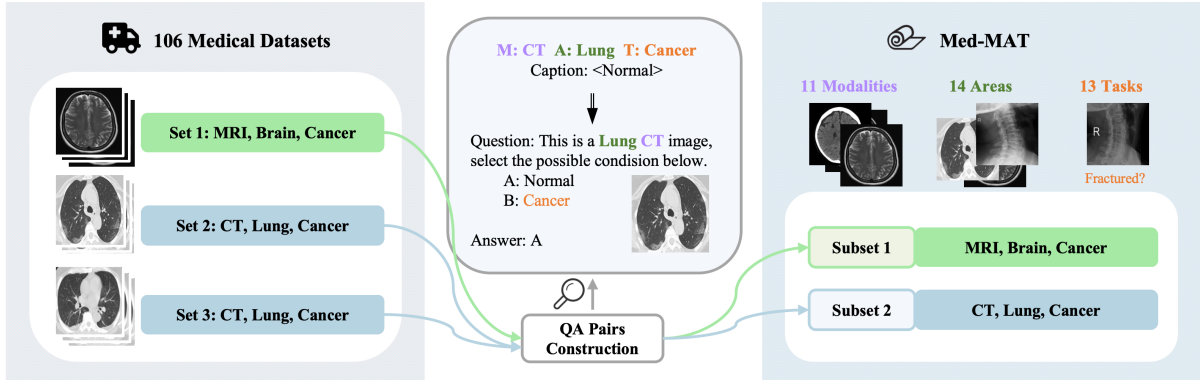


Figure 2: The process of integrating a vast amount of labeled medical image data to create Med-MAT.

same *MAT-Triplet* to create the **Med-MAT** dataset. Ultimately, Med-MAT comprises 53 subsets, encompassing 11 modalities, 14 anatomical regions, and 13 medical tasks, providing a foundation for investigating CG and other generalization methods.

To verify the existence of CG, we designated certain datasets as *Target* data and selected all the *Related* data from Med-MAT that shared the same *MAT-Triplet* with the *Target* data for generalization. In addition, we conducted larger-scale experiments and observed the changes in model generalization performance after deliberately disrupting CG. Ultimately, the experiments demonstrated that MLLMs can leverage CG to understand unseen medical images and CG is one of the key factors driving the generalization observed in multi-task training.

Subsequently, the practical applications of CG and its effects on different backbones were further explored. We found that increasing the volume of CG combinations continuously enhanced the model’s understanding of the *Target* data. While CG’s direct impact on unseen data was not always apparent, CG could assist the model in efficient fitting with limited data by being incorporated into the training data of the *Target*. Furthermore, we discovered that CG exists in different MLLM backbones, underscoring CG’s broad applicability.

Here are the key contributions of our work: 1) A VQA dataset, Med-MAT, has been constructed, providing a platform to explore the generalization of MLLMs on medical images. 2) Through this dataset, we observed that MLLMs can utilize compositional generalization to understand unseen images, demonstrating that this is one of the main forms of generalization for medical MLLMs. 3) Finally, the contribution of CG to understanding medical domains with limited data has been further explored, with its presence across different backbones demonstrating its broad applicability.

2 Med-MAT

Most existing datasets for MLLMs (Zhang et al., 2023c; Li et al., 2024; Chen et al., 2024b), primarily VQA datasets, provide broad coverage but lack attribute annotations for individual samples, which are not suitable for CG exploration. To address this gap, we curated a large collection of image-text pairs to develop Med-MAT, ensuring that each sample is explicitly defined by *MAT-Triplet*. Section 2.1 provides data processing methods; and Section 2.2 presents a pilot experiment.

2.1 Data Processing

Data Construction: Med-MAT contains a total of 106 image-label pair medical datasets, sourced from various medical public challenges or high-quality annotated datasets. All datasets are categorized according to their *MAT-Triplet*, with data having identical elements grouped into a single subset (Figure 2). Labels are manually clustered to ensure that annotations with the same meaning are not repeatedly used. In total, Med-MAT covers 11 medical modalities, 14 anatomical areas, and 13 medical tasks, hoping that it can spread across various medical tasks like a mat. (Data lists are shown in Appendix B)

Data Distribution: All subsets are divided into training and test sets following their original distributions or using a 9:1 ratio. To ensure a fair comparison, each training set is limited to 3,000 samples, with label balance maintained as much as possible. Any subset that cannot meet this requirement is treated as an OOD (out-of-distribution) dataset. For the test sets, we strictly balance the number of samples per label to ensure that the accuracy metric reliably reflects model performance.

QA Pairs Construction: To enable MLLMs to directly train and test on Med-MAT, all image-label

Table 1: Accuracy of different models on In-Distribution Dataset. Within each segment, **bold** highlights the best scores, and underlines indicate the second-best.

Model	02	03	07	08	09	11	13	14	15	16	18	19	21	22	23	25	26	28	30	31	32	33	35	36	37
Baseline	22	47	40	25	26	27	28	24	22	24	25	23	49	26	25	24	49	30	49	21	49	20	25	23	19
Single-task Training	24	49	50	68	<u>65</u>	<u>76</u>	<u>83</u>	<u>53</u>	<u>61</u>	<u>32</u>	<u>29</u>	<u>26</u>	<u>57</u>	<u>53</u>	<u>28</u>	<u>24</u>	<u>57</u>	64	89	60	<u>97</u>	<u>54</u>	<u>29</u>	<u>51</u>	<u>49</u>
Multi-task Training	96	89	80	80	79	97	92	88	76	57	88	74	87	86	93	52	98	72	94	61	100	72	75	60	50

Table 2: Accuracy of different models on Out-Of-Distribution Dataset. **Bold** highlights the best scores.

Model	01	04	05	06	10	12	17	20	24	27	29	34
Baseline	32	25	33	33	48	27	33	13	34	37	31	20
Multi-task Training	39	26	70	31	58	38	61	40	35	41	55	50

paired data were converted into a visual question-answering (VQA) format (Figure 3). Specifically, each subset was manually assigned 6 instructions to guide the MLLM in answering the subset task. For convenience, all samples were converted into single-choice questions with up to four options, and the remaining distractor options were randomly drawn from other labels within the subset. To mitigate potential evaluation biases arising from varying option counts, the ImageWikiQA dataset (Zhang et al., 2024b), a non-medical dataset consisting of single-answer, four-option questions, was incorporated during the training.

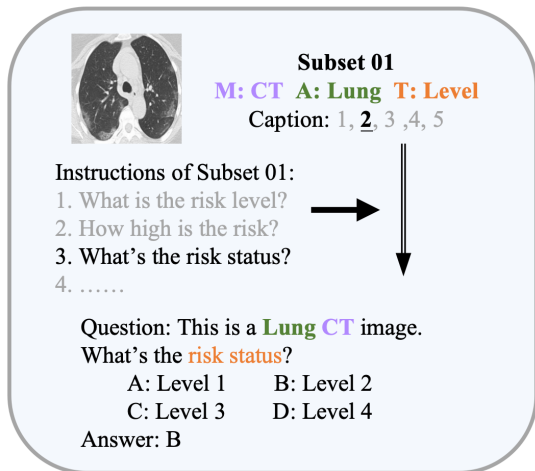


Figure 3: The QA formatting process of Med-MAT.

2.2 A Pilot Study of Data Composition

Experiments Setup: Experiments in this paper mainly focused on classification datasets to explore the model’s combinatorial generalization capabilities across various image types. The base model LLaVA-v1.5-7B-Vicuna (Liu et al., 2023) features a transparent pretraining process and uses very little medical data during training, thereby minimizing the risk of knowledge leakage. By leveraging the flexibility of MLLM, we achieved task switching

and generalization simply by modifying the corresponding prompts, significantly simplifying generalization studies. Each experiment was conducted over 5 epochs using 8 A800 (80GB) GPUs, with a batch size of 32 and a learning rate of 5e-6. Generalization performance was assessed by comparing the model’s accuracy on the *Target* data.

Pilot Study: To explore the benefits of data composition for downstream tasks, all in-distribution (ID) datasets were combined for multi-task training, with single-task training on individual ID datasets serving as the control. The results (Table 1 and 2) showed that multi-task training outperformed single-task training on specific tasks, and also surpassed the baseline in predicting unseen OOD datasets. This suggests that certain data combinations can enhance the model’s classification performance, highlighting the potential for CG. Exploring which combinations provide valuable insights for downstream medical tasks in a promising avenue for further research.

Take-away 1: *Certain data combinations can assist MLLMs in medical classification tasks.*

3 Proof of Concept on CG

To explore whether MLLMs can leverage CG to understand unseen images, controlled variable studies were first conducted using all possible CG combinations to determine if CG exists among the MAT-Triplet (Section 3.1). Subsequently, the number of combinations was increased to explore more generalizable insights, aiming to assess the performance gains of multi-task training (Section 3.2).

3.1 Controlled Variable Study on CG

3.1.1 Experiment Setup

In this section, the existence of CG was explored from a finer perspective, focusing on CG with only

Table 3: Generalization results on classification datasets: "Related Combination" is the training set, "Target Subset" is the goal. Baseline, Baseline+, and Trained represent the model’s accuracy without training, trained on randomly sampled unrelated data, and trained on related data, respectively. Green section indicates successful generalization, while red section denotes failure. The 4 segmented areas represent different Direction Types: fixed modality, fixed area, fixed task, and modality-area paired combinations.

Related Combination		Target Subset	Baseline	Baseline+	Trained
Lung, COVID	Brain, Cancer	Lung, Cancer	25	25	27
Lung, Cancer	Brain, State	Lung, State	47	46	50
Brain, Cancer	Lung, State	Brain, State	33	50	57
Bones, Level	Lung, State	Bones, State	49	53	51
Bones, Level	Brain, State	Bones, State	49	53	72
Bones, Level	Breast, Diseases	Bones, Diseases	37	33	39
Bones, Level	Lung, Diseases	Bones, Diseases	37	33	43
Bones, Level	Chest, Diseases	Bones, Diseases	37	31	43
Bones, State	Breast, Diseases	Bones, Diseases	37	37	43
Bones, State	Lung, Diseases	Bones, Diseases	37	37	43
Bones, State	Chest, Diseases	Bones, Diseases	37	37	41
Lung, COVID	Breast, Diseases	Lung, Diseases	49	48	51
Lung, COVID	Bones, Diseases	Lung, Diseases	49	48	52
Lung, COVID	Chest, Diseases	Lung, Diseases	49	48	51
CT, Cancer	X-ray, COVID	CT, COVID	47	46	72
CT, COVID	X-ray, Diseases	X-ray, COVID	30	21	49
CT, State	X-ray, Diseases	X-ray, State	30	21	46
CT, State	X-ray, Cancer	CT, Cancer	33	28	28
CT, Brain(State)	X-ray, Bones	X-ray, Brain	49	49	91
CT, Brain	X-ray, Lung	X-ray, Brain	49	50	81
CT, Brain(Cancer)	X-ray, Bones	X-ray, Brain	25	51	74
CT, Brain	X-ray, Lung	X-ray, Brain	49	52	52
X-ray, Brain	CT, Lung(State)	CT, Brain(State)	33	50	60
X-ray, Lung	CT, Brain	CT, Lung(Cancer)	25	25	36
X-ray, Lung	CT, Brain(State)	CT, Lung	47	50	81
X-ray, Lung	CT, Brain(Cancer)	CT, Lung	47	50	71
CT, Lung (State)	X-ray, Bones	X-ray, Lung	30	32	28
CT, Lung (State)	X-ray, Brain	X-ray, Lung	30	32	35
CT, Lung (Cancer)	X-ray, Bones	X-ray, Lung	30	32	41
CT, Lung (Cancer)	X-ray, Brain	X-ray, Lung	30	32	42
Der, Skin, Cancer	FP, Fundus, Diseases	Der, Skin, Diseases	25	29	33
Der, Skin, Cancer	OCT, Retine, Diseases	Der, Skin, Diseases	25	29	33
Der, Skin, Diseases	DP, Mouth, Cancer	Der, Skin, Cancer	40	33	63
Der, Skin, Diseases	Mic, Cell, Cancer	Der, Skin, Cancer	40	33	63
DP, Mouth, State	Der, Skin, Cancer	DP, Mouth, Cancer	48	50	52
DP, Mouth, State	Mic, Cell, Cancer	DP, Mouth, Cancer	48	50	55
FP, Fundus, Diseases	Mic, Cell, Level	FP, Fundus, Level	33	36	42
Mic, Cell, Cell identification	FP, Fundus, Level	Mic, Cell, Level	23	33	32
Mic, Cell, Cell identification	Der, Skin, Cancer	Mic, Cell, Cancer	49	50	50
Mic, Cell, Cell identification	DP, Mouth, Cancer	Mic, Cell, Cancer	49	51	62
Mic, Cell, Level	Der, Skin, Cancer	Mic, Cell, Cancer	49	51	52
Mic, Cell, Level	DP, Mouth, Cancer	Mic, Cell, Cancer	49	51	58
Mic, Cell, Cancer	FP, Fundus, Level	Mic, Cell, Level	23	24	27

two elements varying while the third remained constant. For example, we fixed the Modality and examined the CG between Areas and Tasks. Additionally, we identified specific Modality-Area pairs, such as dermoscopy paired consistently with skin, which were treated as a special category. These 4 different fixed formats were classified into distinct *Direction Types*.

Following the setup in Section 2.2, we evaluated the model’s performance on *Target* data. *Baseline* refers to the model without any training, while

Trained refers to the model trained solely on *Related* data. To ensure that our conclusions are not influenced by the amount of training data, we randomly sampled an equal number of data from the *Unrelated* subsets, and this configuration is referred to as *Baseline+*.

3.1.2 Analysis of CG in MLLMs

Results are shown in Table 3 and it can be observed that almost all CG combinations are able to generalize to downstream tasks, highlighting that MLLMs

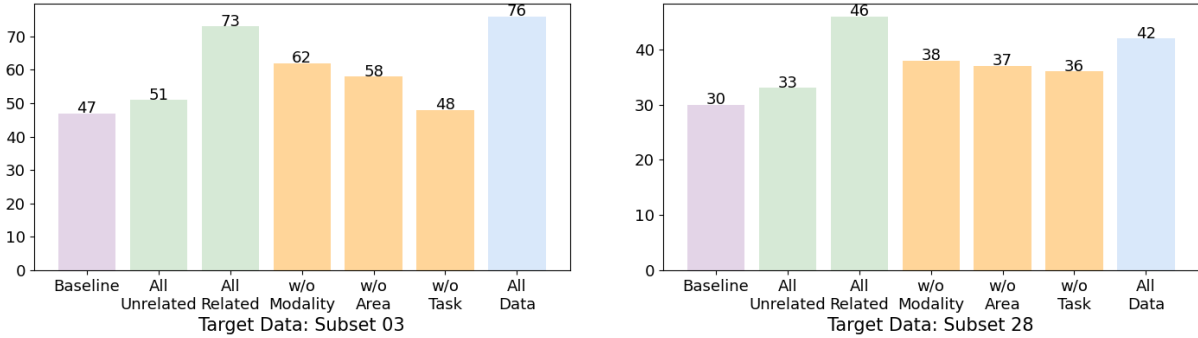


Figure 4: Accuracy results on the Target dataset for various models. ‘All Related/Unrelated’ models are trained on all the related or unrelated datasets of the Target Data. ‘w/o Modality/Area/Task’ are trained on All Related datasets but omit those sharing the same element as the Target Data, to intentionally disrupt CG. ‘All Data’ uses all available training sets. (Note: The Target Data is excluded from training to observe generalization.)

can leverage CG to generalize *Target* data across all Direction Types. Besides that, since this experiment focused solely on two-element tuples, we further investigated three-element tuples in Section 4.3, where we also observed similarly strong generalizations when obtaining MAT-Triplet elements from three different datasets.

Take-away 2: *MLLMs can leverage CG to understand unseen medical images.*

In the *Baseline+* setting, we removed all datasets sharing any MAT-Triplet element with the *Target* data. Consequently, *Baseline+* models perform at near-random levels on the test set, indicating they failed to acquire target-relevant knowledge. This suggests that only datasets related through the MAT-Triplet can help the model learn and generalize to new target tasks.

Take-away 3: *Generalization only arises from MAT-Triplet related medical datasets.*

3.1.3 Analysis of Non-obvious Cases

Some *Trained* models show minimal gains or performance declines, especially in Level or Diseases Identification tasks. The images in the Level Identification are very similar, while the Diseases Identification involves a large number of target labels, both of which require large datasets for training, which may explain the poor performance. To further analyze them, we modified the evaluation scenario to use CG combinations for assisting in *Target* data training with limited samples (Section 4.2).

3.2 Scaling the Combination Number of CG

To ensure the universality of CG, we expanded the number of combination datasets to evaluate its effects on a larger scale. This section explores the following questions: (Q1) While *Meta* CG experiments indicate that *Unrelated* combinations pro-

vide no benefit to *Target* data, can generalization arise when training incorporates more *Unrelated* combinations, simulating a multi-task scenario? (Q2) Previous studies suggest that multi-task training generally promotes better generalization than single-task training. To what extent does this generalization originate from CG?

3.2.1 Experiment Setup

Selection Strategy: To ensure a balanced evaluation of *Related* and *Unrelated* combinations, Subset 03 and Subset 28 were chosen as *Target* datasets because they exhibit the most balanced ratios of *Related* to *Unrelated* subsets (13:11 for Subset 03 and 11:13 for Subset 28), making them ideal for providing a diverse range of compositions in the scale-up experiments.

The baseline was trained on all subsets excluding the *Target* data to evaluate the claim that mixing multi-task data enhances generalization (*All Data*). To construct multiple comparative experiments, models were further trained on either *Related* or *Unrelated* subsets (*All Related / All Unrelated*) to address Q1. For Q2, individual MAT-Triplet elements were systematically removed from the *Related* subsets (*Related w/o Modality / Area / Task*), disrupting CG and assessing the ability to maintain generalization. To ensure consistency, the total data volume in all experiments was limited to 15,000 samples, aligning with the number of ID subsets available after excluding related tasks from Subset 03.

3.2.2 Analysis of Scaling Experiment

Figure 4 illustrates the results. It can be observed that even when we expanded the *Unrelated* combination volumes and increased task diversity, the performance of *All Unrelated* remains close to

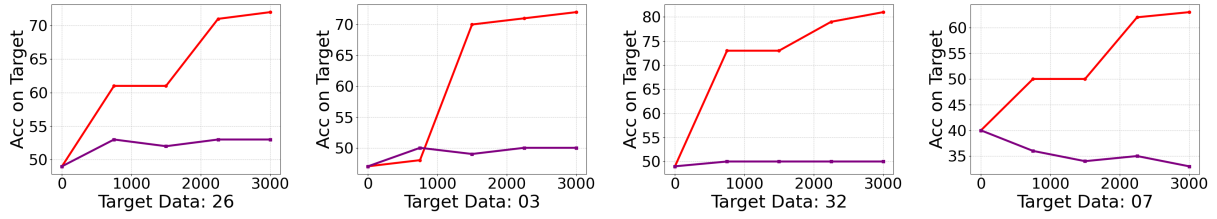


Figure 5: (RQ 1) The curves show how performance on the Target Data improves as the volume of composition datasets increases. The red and purple lines represent training with **Related** and **Unrelated Data**, respectively.

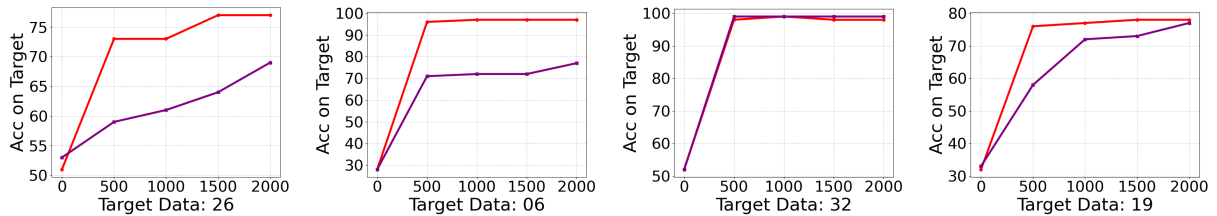


Figure 6: (RQ 2) The curves show how accuracy on Target Data improves as its volume increases with a fixed size of composition data. The red and purple lines represent training with **Related** and **Unrelated Data**, respectively.

the **Baseline**, indicating that these datasets can not support MLLMs to understand the *Target* data.

Take-away 4: *Datasets without MAT-Triplet overlap offer limited benefit for generalization even in the multi-task training scenario (Q1).*

Besides, **w/o Modality / Area / Task** showed significant accuracy drops compared to **All Related**, despite holding the training data volume constant. Notably, **All Related** performs at a level comparable to **All Data**, where all datasets are included in training. This suggests that CG provides significant help for the generalization brought by multi-task training.

Take-away 5: *CG is one of the primary forms of generalization for MLLMs trained on multi-task dataset in medical imaging (Q2).*

4 In-depth Analysis of CG

To further explore the application and applicability of CG, several research questions were proposed in this section. In order to present rich results with minimal consumption of computational resources, specific data Selection Strategies were applied for each question. Here are the research questions:

(RQ 1): How does the quantity of **Related** data affect generalization, and should it be maximized to ensure CG quality?

(RQ 2): Can CG combinations help the model efficiently fit Target data when only a small amount of Target data is available?

(RQ 3): Previous studies demonstrated that CG exists between two MAT-Triplet elements, does CG still exist if the three MAT-Triplet elements come

from three different datasets?

(RQ 4): Does CG exist between images from Detection tasks and Classification tasks?

(RQ 5): Can different MLLM backbones leverage CG to interpret unseen medical images?

4.1 The Relationship Between CG Performance and Data Volume

Selection Strategy: This section focuses on examining how the data volume of **Related** combinations influences generalization. To highlight the generalization trends, the combinations with strong generalization results were selected from the main experiments. For fairness, we chose the combinations across four types where **Trained** results exceeded both **Baseline** and **Baseline+** by at least 10. If multiple combinations meet the criteria, a random seed of 42 was used to determine the selection.

In this experiment, the amount of combination data was gradually increased (from 0 to 750, 1500, 2250, and 3000), and the trend of the model’s accuracy on *Target* data after training was observed. The experimental results are shown in Figure 5, where the red line represents the accuracy curve gained from **Related** combinations, and the purple line represents the gain from **Unrelated** combinations. Models trained on **Related** combinations demonstrate strong performance across all four Target data sets. As the data volume of **Related** combinations increases, the model’s understanding of *Target* data improves consistently.

Take-away 6: *Generalization effect improves with increasing CG combination’s volume. (RQ 1)*

Table 4: Generalization results from 3 datasets providing different elements of MAT-Triplet (RQ 3). "Related Combination" is the training set, "Target Subset" is the goal. Baseline, and Trained represent the model's accuracy without training and trained on *Related* data, respectively. Green section indicates successful generalization, while red section denotes failure.

Related Combination			Target Subset	Baseline	Trained
CT - Subset02	Brain - Subset22	Cancer - Subset07	CT, Brain, Cancer	28	26
CT - Subset03	Brain - Subset22	Cancer - Subset21	CT, Brain, Cancer	28	25
CT - Subset02	Brain - Subset22	State - Subset09	CT, Brain, State	33	64
CT - Subset03	Brain - Subset22	State - Subset26	CT, Brain, State	33	70
X-ray - Subset25	Lung - Subset03	Diseases - Subset02	X-ray, Lung, Diseases	30	45
X-ray - Subset26	Lung - Subset03	Diseases - Subset02	X-ray, Lung, Diseases	30	38
X-ray - Subset26	Lung - Subset03	Diseases - Subset08	X-ray, Lung, Diseases	30	44
X-ray - Subset26	Breast - Subset24	Diseases - Subset02	X-ray, Breast, Diseases	31	32
X-ray - Subset28	Breast - Subset24	Diseases - Subset08	X-ray, Breast, Diseases	31	52

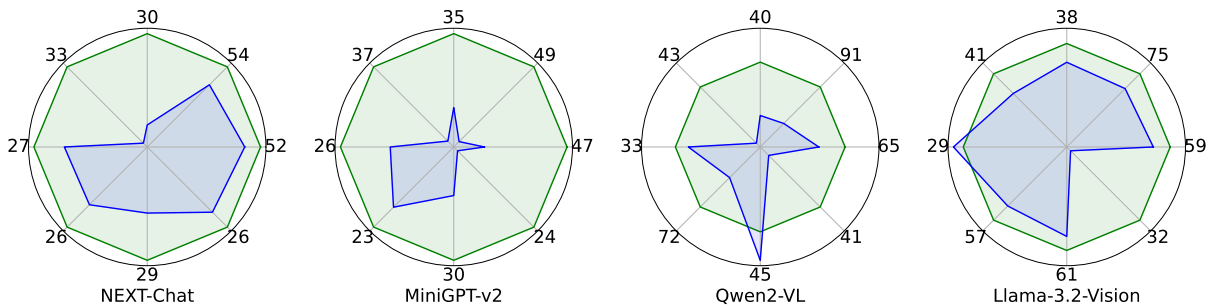


Figure 7: The accuracy of different backbones: The blue line represents the untrained model, and the green line represents the CG-trained model. All data are scaled based on the accuracy of CG combinations, which is displayed at each corner (details in Appendix A.1 and A.2).

4.2 Achieving Data-Efficient Training through CG

Selection Strategy: This experiment evaluates how CG aids training and dataset fitting with limited *Target* data. To highlight performance trends, four combinations with poor generalization (marked in red in Table 3) were selected across the four Direction Types, ensuring both models in the control group started with similar baseline accuracies. When multiple poor-performing combinations existed within a Direction Type, the more challenging datasets were chosen based on Table 1 to better observe potential improvements.

In this experiment, the amount of *Target* data was progressively increased (from 0 to 500, 1000, 1500, and 2000), and a fixed number of combination data were incorporated during training. Figure 6 displays the results, with red lines showing accuracy gains from *Related* combination and purple lines from *Unrelated* ones. It can be observed that training with *Related* combination data reaches peak performance more quickly, demonstrating another form of CG. Therefore, although CG performs poorly on these data due to task characteristics, it still helps the model quickly adapt with only

a small amount of *Target* data.

Take-away 7: Although CG does not always provide direct generalization gains, it can help *Target* data achieve data-efficient training. (RQ 2)

4.3 CG with All MAT-Triplet Elements from Different Sources

In previous controlled experiments (Section 3.1), one element of the MAT-Triplet was kept constant while CG was explored in the remaining two elements. To ensure that all the 3 MAT-Triplet elements of the target data originated from three distinct datasets, additional experiments were conducted to further validate the effectiveness of CG. For these experiments, all possible combinations meeting the criteria in Med-MAT were selected (**Selection Strategy**). The results presented in Table 4 demonstrate that most combinations can effectively generalize to the *Target* data.

Take-away 8: CG remains effective when all elements come from different datasets (RQ 3).

4.4 Detection-Capable MLLMs can Leverage Detection Data for CG

Previous studies (Ren et al., 2024; Wang et al., 2025) have demonstrated that jointly training clas-

sification and detection tasks can mutually enhance their performance. Building on this, we explored CG within this context. To ensure comprehensive conclusions, we conducted experiments using NextChat and MiniGPT-v2, which represent the two mainstream approaches for MLLMs to perform segmentation tasks. The former treats bounding boxes as embeddings and decodes them into coordinates using an additional visual decoder, while the latter processes coordinate points as special text tokens and generates bounding box coordinates directly as output text. The final results (Figure 7) show that all CG combinations demonstrated the model’s successful utilization of detection data for CG to the *Target* data.

Take-away 9: *MLLMs can combine knowledge from detection tasks with classification tasks to improve classification accuracy (RQ 4).*

4.5 CG Exists Across Different MLLM Backbones

LLaVA was selected as the baseline because its training data and processes are publicly available, ensuring minimal exposure to medical images and preventing bias in the integration of medical image knowledge into the MLLM. To verify that CG is not limited to a single framework, we also selected subsets for experiments on Qwen2-VL-7B (Wang et al., 2024a) and Llama3.2-11B-Vision (Meta AI, 2024). The results in Figure 7 demonstrate CG effects similar to those observed in the LLaVA.

Take-away 10: *CG persists across different MLLM backbones (RQ 5).*

5 Related Work

Medical MLLMs: Recently, adapting MLLMs to medical tasks has gained prominence due to their success in capturing complex visual features. Current MLLMs typically pair a visual encoder with a text-only LLM, aligning image data with language understanding. Such as Med-Flamingo (Moor et al., 2023) and Med-PaLM (Tu et al., 2024), fine-tuned general multimodal models and achieved notable results. Med-Flamingo enhanced OpenFlamingo-9B (Chen et al., 2024a) with medical data, while Med-PaLM adapted PaLM-E (Driess et al., 2023) using 1 million data points. Similarly, LLaVA-Med (Li et al., 2024), Med-Gemini (Saab et al., 2024), and HuatuoGPT-Vision (Chen et al., 2024b) utilized specialized datasets and instruction tuning to refine medical VQA tasks.

Generalization on Medical Imaging: Generalization in medical imaging (Matta et al., 2024) has been extensively studied. Early methods utilized data manipulation techniques, such as data augmentation (Li et al., 2022; Zhang et al., 2022), to enhance model generalization on unseen medical data by adapting to varying distributions. Later approaches focused on representation learning (LeKhac et al., 2020), preserving essential image information to enable models to handle more complex scenarios. Additionally, some studies (Ren et al., 2024) explore multiple aspects of medical image processing, examining how classification and segmentation tasks can mutually benefit each other.

Detection with MLLMs: MiniGPT-4 (Zhu et al., 2023) and LLaVA (Liu et al., 2023) enhance LLMs by fine-tuning models on synthetic multimodal instruction data. However, these models are limited to image and text inputs and cannot generate detection bounding boxes or segmentation masks. Recent works have addressed these limitations using various strategies, such as encoding regions as features to allow models to accept regions as input (Zhang et al., 2023b), representing object bounding box coordinates with text tokens (Wang et al., 2024c; Peng et al., 2023; Chen et al., 2023b), and employing unique identifiers for task instructions to improve learning efficiency. Additionally, some approaches introduce special tokens to represent images and use their hidden states to decode position information (Zhang et al., 2023a, 2024a).

6 Conclusion

To explore whether MLLMs can leverage CG to generalize unseen medical data, we constructed the Med-MAT dataset as the research platform for generalization experiments. The results confirmed the existence of CG and identified it as one of the primary factors behind the generalization capability of MLLMs in multi-task learning. Subsequent experiments demonstrated that increasing the volume of CG combinations consistently improved their effectiveness. Furthermore, CG enables medical tasks to efficiently fit with limited data, reducing dependence on the volume of training data. Importantly, CG is present across various MLLM backbones and can even facilitate generalization using data from tasks such as detection, underscoring its broad applicability.

Limitations

The experiment confirms that MLLMs can use CG to understand unseen medical images and achieve data-efficient training. However, as shown in the results in 3.2, even after disrupting CG, the model's generalization performance declines but still maintains some level of effectiveness. Thus, CG represents only one form of generalization for MLLMs in medical imaging. To support the exploration of other generalization mechanisms, we will make datasets publicly available according to the license.

This study is focused exclusively on medical scenarios, but we believe that similar generalization effects may also apply in other multimodal tasks. Additionally, more granular medical generalization strategies, such as leveraging existing pneumonia data to generalize the detection of newly emerging types of pneumonia, are also promising areas for further investigation.

Potential Risks

Our research focuses on the compositional generalization of MLLMs on medical images, using data sourced from medical challenges and open-source datasets. However, further experiments are needed to mitigate potential risks when deploying this concept in real-world medical settings.

References

- Andrea Acevedo, Anna Merino, Santiago Alf rez,  ngel Molina, Laura Bold , and Jos  Rodellar. 2020. A dataset of microscopic peripheral blood cell images for development of automatic recognition systems. *Data in brief*, 30:105474.
- Walid Al-Dhabyani, Mohammed Gomaa, Hussien Khaled, and Aly Fahmy. 2020. Dataset of breast ultrasound images. *Data in brief*, 28:104863.
- Shams Nafisa Ali, Md. Tazuddin Ahmed, Joydip Paul, Tasnim Jahan, S. M. Sakeef Sani, Nawshaba Noor, and Taufiq Hasan. 2022. Monkeypox skin lesion detection using deep learning models: A preliminary feasibility study. *arXiv preprint arXiv:2207.03342*.
- Sharib Ali, Barbara Braden, Dominique Lamarque, Stefano Realdon, Adam Bailey, Renato Cannizzaro, Noha Ghatwary, Jens Rittscher, Christian Daul, and James East. 2020. [Endoscopy disease detection and segmentation \(edd2020\)](#).
- MD Anouk Stein, Carol Wu, Chris Carr, George Shih, Jamie Dulkowski, kalpathy, Leon Chen, Luciano Prevedello, MD Marc Kohli, Mark McDonald, Peter, Phil Culliton, Safwan Halabi MD, and Tian Xia. 2018. Rsna pneumonia detection challenge. <https://kaggle.com/competitions/rsna-pneumonia-detection-challenge>. Kaggle.
- Will Arevalo. 2020. Chexpert v1.0 small. <https://www.kaggle.com/datasets/willarevalo/chexpert-v10-small>. Kaggle.
- A Asraf and Z Islam. 2021. Covid19, pneumonia and normal chest x-ray pa dataset. mendeley data v1 (2021).
- Francisco Jos  Fumero Batista, Tinguaro Diaz-Aleman, Jose Sigut, Silvia Alayon, Rafael Arnay, and Denisse Angel-Pereira. 2020. [Rim-one dl: A unified retinal image database for assessing glaucoma using deep learning](#). *Image Analysis & Stereology*, 39(3):161–167.
- Dev Batra. 2024. Fracture detection using x-ray images. <https://www.kaggle.com/datasets/devbatrax/fracture-detection-using-x-ray-images>. Kaggle.
- Veronica Elisa Castillo Ben tez, Ingrid Castro Matto, Julio C sar Mello Rom n, Jos  Luis V zquez Noguera, Miguel Garc a-Torres, Jordan Ayala, Diego P Pinto-Roa, Pedro E Gardel-Sotomayor, Jacques Facon, and Sebastian Alberto Grillo. 2021. Dataset from fundus images for the study of diabetic retinopathy. *Data in brief*, 36:107068.
- BenO, jlJones, Kumar H, Meg Risdal, MRao, Vadim Sherman, Vipul, Wendy Kan, and Yau Ben-Or. 2017. Intel & mobileodt cervical cancer screening. <https://kaggle.com/competitions/intel-mobileodt-cervical-cancer-screening>. Kaggle.
- Jorge Bernal, F Javier S nchez, Gloria Fern ndez-Esparrach, Debora Gil, Cristina Rodr guez, and Fernando Vilari o. 2015. Wm-dova maps for accurate polyp highlighting in colonoscopy: Validation vs. saliency maps from physicians. *Computerized medical imaging and graphics*, 43:99–111.
- Bukun. 2019. Breast cancer histopathological database (breakhis). <https://www.kaggle.com/datasets/ambarish/breakhis>. Kaggle.
- Olivia Cardozo, Verena Ojeda, Rodrigo Parra, Julio C sar Mello-Rom n, Jos  Luis V zquez Noguera, Miguel Garc a-Torres, Federico Divina, Sebastian A. Grillo, Cynthia Villalba, Jacques Facon, Veronica Elisa Castillo Ben tez, Ingrid Castro Matto, and Diego Aquino-Br tez. 2023. [Dataset of fundus images for the diagnosis of ocular toxoplasmosis](#). *Data in Brief*, 48:109056.
- Ling-Ping Cen, Jie Ji, Jian-Wei Lin, Si-Tong Ju, Hong-Jie Lin, Tai-Ping Li, Yun Wang, Jian-Feng Yang, Yu-Fen Liu, Shaoying Tan, et al. 2021. Automatic detection of 39 fundus diseases and conditions in retinal photographs using deep neural networks. *Nature communications*, 12(1):4828.

- Delong Chen, Jianfeng Liu, Wenliang Dai, and Baoyuan Wang. 2024a. Visual instruction tuning with polite flamingo. In *Proceedings of the AAAI Conference on Artificial Intelligence*, volume 38, pages 17745–17753.
- Jun Chen, Deyao Zhu, Xiaoqian Shen, Xiang Li, Zechun Liu, Pengchuan Zhang, Raghuraman Krishnamoorthi, Vikas Chandra, Yunyang Xiong, and Mohamed Elhoseiny. 2023a. Minigpt-v2: large language model as a unified interface for vision-language multi-task learning. *arXiv preprint arXiv:2310.09478*.
- Junying Chen, Ruyi Ouyang, Anningzhe Gao, Shunian Chen, Guiming Hardy Chen, Xidong Wang, Ruifei Zhang, Zhenyang Cai, Ke Ji, Guangjun Yu, et al. 2024b. Huatuogpt-vision, towards injecting medical visual knowledge into multimodal llms at scale. *arXiv preprint arXiv:2406.19280*.
- Keqin Chen, Zhao Zhang, Weili Zeng, Richong Zhang, Feng Zhu, and Rui Zhao. 2023b. Shikra: Unleashing multimodal llm’s referential dialogue magic. *arXiv preprint arXiv:2306.15195*.
- Pingjun Chen. 2018. Knee osteoarthritis severity grading dataset. *Mendeley Data*, 1(10.17632).
- Muhammad E. H. Chowdhury, Tawsifur Rahman, Amith Khandakar, Rashid Mazhar, Muhammad Abdul Kadir, Zaid Bin Mahbub, Khandakar Reajul Islam, Muhammad Salman Khan, Atif Iqbal, Nasser Al Emadi, Mamun Bin Ibne Reaz, and Mohammad Tariqul Islam. 2020. Can ai help in screening viral and covid-19 pneumonia? *IEEE Access*, 8:132665–132676.
- Noel Codella, Veronica Rotemberg, Philipp Tschandl, M Emre Celebi, Stephen Dusza, David Gutman, Brian Helba, Aadi Kalloo, Konstantinos Liopyris, Michael Marchetti, et al. 2019. Skin lesion analysis toward melanoma detection 2018: A challenge hosted by the international skin imaging collaboration (isic). *arXiv preprint arXiv:1902.03368*.
- Noel CF Codella, David Gutman, M Emre Celebi, Brian Helba, Michael A Marchetti, Stephen W Dusza, Aadi Kalloo, Konstantinos Liopyris, Nabin Mishra, Harald Kittler, et al. 2018. Skin lesion analysis toward melanoma detection: A challenge at the 2017 international symposium on biomedical imaging (isbi), hosted by the international skin imaging collaboration (isic). In *2018 IEEE 15th international symposium on biomedical imaging (ISBI 2018)*, pages 168–172. IEEE.
- Marc Combalia, Noel CF Codella, Veronica Rotemberg, Brian Helba, Veronica Vilaplana, Ofer Reiter, Cristina Carrera, Alicia Barreiro, Allan C Halpern, Susana Puig, et al. 2019. Bcn20000: Dermoscopic lesions in the wild. *arXiv preprint arXiv:1908.02288*.
- Will Cukierski. 2018. Histopathologic cancer detection. <https://kaggle.com/competitions/histopathologic-cancer-detection>. Kaggle.
- Training Data. 2023. Computed tomography of the brain. <https://www.kaggle.com/datasets/trainingdatapro/computed-tomography-ct-of-the-brain>. Kaggle.
- Coen de Vente, Koenraad A. Vermeer, Nicolas Jaccard, He Wang, Hongyi Sun, Firas Khader, Daniel Truhn, Temirgali Aimyshev, Yerkebulan Zhanibekuly, Tien-Dung Le, Adrian Galdran, Miguel Ángel González Ballester, Gustavo Carneiro, Devika R G, Hrishikesh P S, Densen Puthussery, Hong Liu, Zekang Yang, Satoshi Kondo, Satoshi Kasai, Edward Wang, Ashritha Durvasula, Jónathan Heras, Miguel Ángel Zapata, Teresa Araújo, Guilherme Aresta, Hrvoje Bogunović, Mustafa Arikian, Yeong Chan Lee, Hyun Bin Cho, Yoon Ho Choi, Abdul Qayyum, Imran Razzak, Bram van Ginneken, Hans G. Lemij, and Clara I. Sánchez. 2023. Airogs: Artificial intelligence for robust glaucoma screening challenge. *arXiv preprint arXiv:2302.01738*.
- Danny Driess, Fei Xia, Mehdi SM Sajjadi, Corey Lynch, Aakanksha Chowdhery, Brian Ichter, Ayzaan Wahid, Jonathan Tompson, Quan Vuong, Tianhe Yu, et al. 2023. Palm-e: An embodied multimodal language model. *arXiv preprint arXiv:2303.03378*.
- Fernando Feltrin. 2022. Brain tumor mri images 17 classes. <https://www.kaggle.com/datasets/fernando2rad/brain-tumor-mri-images-17-classes>. Kaggle.
- Mohammad Fraiwan, Ziad Audat, Luay Fraiwan, and Tarek Manasreh. 2022. Using deep transfer learning to detect scoliosis and spondylolisthesis from x-ray images. *Plos one*, 17(5):e0267851.
- Huazhu Fu, Fei Li, José Ignacio Orlando, Hrvoje Bogunović, Xu Sun, Jingan Liao, Yanwu Xu, Shaochong Zhang, and Xiulan Zhang. 2019. *Palm: Pathologic myopia challenge*.
- Ioannis Giotis, Nynke Molders, Sander Land, Michael Biehl, Marcel F Jonkman, and Nicolai Petkov. 2015. Med-node: A computer-assisted melanoma diagnosis system using non-dermoscopic images. *Expert systems with applications*, 42(19):6578–6585.
- Haifan Gong, Guanqi Chen, Ranran Wang, Xiang Xie, Mingzhi Mao, Yizhou Yu, Fei Chen, and Guanbin Li. 2021. Multi-task learning for thyroid nodule segmentation with thyroid region prior. In *2021 IEEE 18th international symposium on biomedical imaging (ISBI)*, pages 257–261. IEEE.
- Haifan Gong, Jiaxin Chen, Guanqi Chen, Haofeng Li, Fei Chen, and Guanbin Li. 2022. Thyroid region prior guided attention for ultrasound segmentation of thyroid nodules. *Computers in Biology and Medicine*, 106389:1–12.
- Shivanand Gornale and Pooja Patravali. 2020. *Digital knee x-ray images*.

- Matthew Groh, Caleb Harris, Luis Soenksen, Felix Lau, Rachel Han, Aerin Kim, Arash Koochek, and Omar Badri. 2021. Evaluating deep neural networks trained on clinical images in dermatology with the fitzpatrick 17k dataset. In *Proceedings of the IEEE/CVF Conference on Computer Vision and Pattern Recognition*, pages 1820–1828.
- David Gutman, Noel CF Codella, Emre Celebi, Brian Helba, Michael Marchetti, Nabin Mishra, and Allan Halpern. 2016. Skin lesion analysis toward melanoma detection: A challenge at the international symposium on biomedical imaging (isbi) 2016, hosted by the international skin imaging collaboration (isic). *arXiv preprint arXiv:1605.01397*.
- Saba Hesaraki. 2022. Breast ultrasound images dataset (busi). <https://www.kaggle.com/datasets/sabahesaraki/breast-ultrasound-images-dataset>. Kaggle.
- Md Nazmul Islam, Mehedi Hasan, Md Kabir Hossain, Md Golam Rabiul Alam, Md Zia Uddin, and Ahmet Soylu. 2022a. Vision transformer and explainable transfer learning models for auto detection of kidney cyst, stone and tumor from ct-radiography. *Scientific Reports*, 12(1):1–14.
- Towhidul Islam, Mohammad Arafat Hussain, Forhad Uddin Hasan Chowdhury, and B M Riazul Islam. 2022b. A web-scraped skin image database of monkeypox, chickenpox, smallpox, cowpox, and measles. *bioRxiv* 2022.08.01.502199.
- Stefan Jaeger, Sema Candemir, Sameer Antani, Yi-Xiang J Wang, Pu-Xuan Lu, and George Thoma. 2014. Two public chest x-ray datasets for computer-aided screening of pulmonary diseases. *Quantitative imaging in medicine and surgery*, 4(6):475.
- Debesh Jha, Pia H Smedsrud, Michael A Riegler, Pål Halvorsen, Thomas de Lange, Dag Johansen, and Håvard D Johansen. 2020. Kvasir-seg: A segmented polyp dataset. In *MultiMedia Modeling: 26th International Conference, MMM 2020, Daejeon, South Korea, January 5–8, 2020, Proceedings, Part II 26*, pages 451–462. Springer.
- Kai Jin, Xingru Huang, Jingxing Zhou, Yunxiang Li, Yan Yan, Yibao Sun, Qianni Zhang, Yaqi Wang, and Juan Ye. 2022. Fives: A fundus image dataset for artificial intelligence based vessel segmentation. *Scientific data*, 9(1):475.
- JR2NGB. 2019. Cataract dataset. <https://www.kaggle.com/datasets/jr2n gb/cataractdataset>. Kaggle.
- Nur Karaca. 2022. Nlm montgomery cxr set. <https://www.kaggle.com/datasets/nurkaraca/nlm-montgomerycxrset>. Kaggle.
- Karthik, Maggie, and Sohier Dane. 2019. Aptos 2019 blindness detection. <https://kaggle.com/competitions/aptos2019-blindness-detection>. Kaggle.
- Andrey Katanskiy. 2019. Skin cancer isic. <https://www.kaggle.com/datasets/nodoubttome/skin-cancer9-classesisic>. Kaggle.
- Jakob Nikolas Kather, Niels Halama, and Alexander Marx. 2018. 100,000 histological images of human colorectal cancer and healthy tissue.
- Daniel Kermany. 2018. Labeled optical coherence tomography (oct) and chest x-ray images for classification. *Mendeley data*.
- Felipe Campos Kitamura. 2018. Head ct - hemorrhage.
- Jorge F Lazo, Benoit Rosa, Michele Catellani, Matteo Fontana, Francesco A Mistretta, Gennaro Musi, Ottavio de Cobelli, Michel de Mathelin, and Elena De Momi. 2023. Semi-supervised bladder tissue classification in multi-domain endoscopic images. *IEEE Transactions on Biomedical Engineering*.
- Trang Le, Casper F Winsnes, Ulrika Axelsson, Hao Xu, Jayasankar Mohanakrishnan Kaimal, Diana Mahdessian, Shubin Dai, Ilya S Makarov, Vladislav Ostankovich, Yang Xu, et al. 2022. Analysis of the human protein atlas weakly supervised single-cell classification competition. *Nature methods*, 19(10):1221–1229.
- Phuc H Le-Khac, Graham Healy, and Alan F Smeaton. 2020. Contrastive representation learning: A framework and review. *Ieee Access*, 8:193907–193934.
- Rebecca Sawyer Lee, Francisco Gimenez, Assaf Hoogi, Kanae Kawai Miyake, Mia Gorovoy, and Daniel L Rubin. 2017. A curated mammography data set for use in computer-aided detection and diagnosis research. *Scientific data*, 4(1):1–9.
- Sangjune L Lee, Poonam Yadav, Yin Li, Jason J Meudt, Jessica Strang, Dustin Hebel, Alyx Alfson, Stephanie J Olson, Tera R Kruser, Jennifer B Smilowitz, et al. 2024. Dataset for gastrointestinal tract segmentation on serial mris for abdominal tumor radiotherapy. *Data in Brief*, page 111159.
- Chunyu Li, Cliff Wong, Sheng Zhang, Naoto Usuyama, Haotian Liu, Jianwei Yang, Tristan Naumann, Hoifung Poon, and Jianfeng Gao. 2024. Llava-med: Training a large language-and-vision assistant for biomedicine in one day. *Advances in Neural Information Processing Systems*, 36.
- Yuanpeng Li, Liang Zhao, Jianyu Wang, and Joel Hestness. 2019. Compositional generalization for primitive substitutions. *arXiv preprint arXiv:1910.02612*.
- Yuexiang Li, Nanjun He, and Yawen Huang. 2022. Single domain generalization via spontaneous amplitude spectrum diversification. In *MICCAI Workshop on Resource-Efficient Medical Image Analysis*, pages 32–41. Springer.

- Jie Lian, Jingyu Liu, Shu Zhang, Kai Gao, Xiaoqing Liu, Dingwen Zhang, and Yizhou Yu. 2021. A structure-aware relation network for thoracic diseases detection and segmentation. *IEEE Transactions on Medical Imaging*, 40(8):2042–2052.
- Xiao Liang. 2021. Adam dataset. <https://www.kaggle.com/datasets/xiaoliang2121/adamdataset>. Kaggle.
- Haotian Liu, Chunyuan Li, Qingyang Wu, and Yong Jae Lee. 2023. Visual instruction tuning.
- Jacob A Macdonald, Zhe Zhu, Brandon Konkel, and Mazurowski. 2020. Siim-acr pneumothorax segmentation. <https://doi.org/10.5281/zenodo.7774566>. Zenodo.
- K Scott Mader. 2017. Mias mammography. <https://www.kaggle.com/datasets/kmader/mias-mammography>. Kaggle.
- Salman Maqbool, Aqsa Riaz, Hasan Sajid, and Osman Hasan. 2020. m2caiseg: Semantic segmentation of laparoscopic images using convolutional neural networks. *arXiv preprint arXiv:2008.10134*.
- Christian Matek, Sebastian Krappe, Christian Münzenmayer, Torsten Haferlach, and Carsten Marr. 2021. An expert-annotated dataset of bone marrow cytology in hematologic malignancies. *The Cancer Imaging Archive*.
- Sarah Matta, Mathieu Lamard, Philippe Zhang, Alexandre Le Guilcher, Laurent Borderie, Béatrice Cochener, and Gwenolé Quellec. 2024. A systematic review of generalization research in medical image classification. *arXiv preprint arXiv:2403.12167*.
- Teresa Mendonca, M Celebi, T Mendonca, and J Marques. 2015. Ph2: A public database for the analysis of dermoscopic images. *Dermoscopy image analysis*.
- Meta AI. 2024. Llama 3.2: Revolutionizing edge ai and vision with open, customizable models. <https://ai.meta.com/blog/llama-3-2-connect-2024-vision-edge-mobile-devices/>.
- Shentong Mo and Paul Pu Liang. 2024. Multimed: Massively multimodal and multitask medical understanding. *arXiv preprint arXiv:2408.12682*.
- Paul Mooney. 2017. Blood cell images. <https://www.kaggle.com/datasets/paultimothymooney/blood-cells>. Kaggle.
- Michael Moor, Qian Huang, Shirley Wu, Michihiro Yasunaga, Yash Dalmia, Jure Leskovec, Cyril Zakkka, Eduardo Pontes Reis, and Pranav Rajpurkar. 2023. Med-flamingo: a multimodal medical few-shot learner. In *Machine Learning for Health (ML4H)*, pages 353–367. PMLR.
- Loris Nanni, Michelangelo Paci, Florentino Luciano Caetano dos Santos, Heli Skottman, Kati Juuti-Uusitalo, and Jari Hyttinen. 2016. Texture descriptors ensembles enable image-based classification of maturation of human stem cell-derived retinal pigmented epithelium. *PLoS One*, 11(2):e0149399.
- Hieu T Nguyen, Ha Q Nguyen, Hieu H Pham, Khanh Lam, Linh T Le, Minh Dao, and Van Vu. 2023. Vindr-mammo: A large-scale benchmark dataset for computer-aided diagnosis in full-field digital mammography. *Scientific Data*, 10(1):277.
- Masoud Nickparvar. 2021a. Brain tumor mri dataset. <https://www.kaggle.com/datasets/masoudnickparvar/brain-tumor-mri-dataset>. Kaggle.
- Msoud Nickparvar. 2021b. Brain tumor mri dataset.
- Nikita Orlov, Wayne Chen, David Eckley, Tomasz Macura, Lior Shamir, Elaine Jaffe, and Ilya Goldberg. 2010a. Automatic classification of lymphoma images with transform-based global features. *IEEE transactions on information technology in biomedicine : a publication of the IEEE Engineering in Medicine and Biology Society*, 14:1003–13.
- Nikita Orlov, Wayne Chen, David Eckley, Tomasz Macura, Lior Shamir, Elaine Jaffe, and Ilya Goldberg. 2010b. Automatic classification of lymphoma images with transform-based global features. *IEEE transactions on information technology in biomedicine : a publication of the IEEE Engineering in Medicine and Biology Society*, 14:1003–13.
- Silvia Ovreiu, Elena-Anca Paraschiv, and Elena Ovreiu. 2021. Deep learning & digital fundus images: Glaucoma detection using densenet. In *2021 13th international conference on electronics, computers and artificial intelligence (ECAI)*, pages 1–4. IEEE.
- Andre GC Pacheco, Gustavo R Lima, Amanda S Salomao, Breno Krohling, Igor P Biral, Gabriel G de Angelo, Fábio CR Alves Jr, José GM Esgario, Alana C Simora, Pedro BC Castro, et al. 2020. Pad-ufes-20: A skin lesion dataset composed of patient data and clinical images collected from smartphones. *Data in brief*, 32:106221.
- Sachin Panchal, Ankita Naik, Manesh Kokare, Samiksha Pachade, Rushikesh Naigaonkar, Prerana Phadnis, and Archana Bhanghe. 2023. Retinal fundus multi-disease image dataset (rfmid) 2.0: a dataset of frequently and rarely identified diseases. *Data*, 8(2):29.
- Zhiliang Peng, Wenhui Wang, Li Dong, Yaru Hao, Shaohan Huang, Shuming Ma, and Furu Wei. 2023. Kosmos-2: Grounding multimodal large language models to the world. *arXiv preprint arXiv:2306.14824*.
- H Hieu Pham, T Thanh Tran, and Ha Quy Nguyen. 2022. Vindr-pcxr: An open, large-scale pediatric chest x-ray dataset for interpretation of common thoracic diseases. *PhysioNet (version 1.0. 0)*, 10:2.

- Hieu Huy Pham, H Nguyen Trung, and Ha Quy Nguyen. 2021. Vindr-spinexr: A large annotated medical image dataset for spinal lesions detection and classification from radiographs. *PhysioNet*.
- Konstantin Pogorelov, Kristin Ranheim Randel, Thomas de Lange, Sigrun Losada Eskeland, Carsten Griwodz, Dag Johansen, Concetto Spampinato, Mario Taschwer, Mathias Lux, Peter Thelin Schmidt, Michael Riegler, and Pål Halvorsen. 2017a. Nerthus: A bowel preparation quality video dataset. In *Proceedings of the 8th ACM on Multimedia Systems Conference, MMSys'17*, pages 170–174, New York, NY, USA. ACM.
- Konstantin Pogorelov, Kristin Ranheim Randel, Carsten Griwodz, Sigrun Losada Eskeland, Thomas de Lange, Dag Johansen, Concetto Spampinato, Duc-Tien Dang-Nguyen, Mathias Lux, Peter Thelin Schmidt, Michael Riegler, and Pål Halvorsen. 2017b. Kvasir: A multi-class image dataset for computer aided gastrointestinal disease detection. In *Proceedings of the 8th ACM on Multimedia Systems Conference, MMSys'17*, pages 164–169, New York, NY, USA. ACM.
- Praveen. 2019. Coronahack chest x-ray dataset. <https://www.kaggle.com/datasets/praveengovi/coronahack-chest-xraydataset>. Kaggle.
- Pavle Prentasic, Sven Loncaric, Zoran Vatauvuk, Goran Bencic, Marko Subasic, Tomislav Petković, Lana Dujmovic, Maja Malenica Ravlic, Nikolina Budimlija, and Rašeljka Tadić. 2013. Diabetic retinopathy image database(dridb): A new database for diabetic retinopathy screening programs research. pages 711–716.
- Xianbiao Qi, Guoying Zhao, Jie Chen, and Matti Pietikäinen. 2016. Hep-2 cell classification: The role of gaussian scale space theory as a pre-processing approach. *Pattern Recognition Letters*, 82:36–43.
- Raddar. 2019. Chest x-rays (indiana university). https://www.kaggle.com/datasets/raddar/chest-xrays-indiana-university?select=indiana_reports.csv. Kaggle.
- Tawsifur Rahman, Amith Khandakar, Muhammad Abdul Kadir, Khandaker Rejaul Islam, Khandakar F Islam, Rashid Mazhar, Tahir Hamid, Mohammad Tariqul Islam, Saad Kashem, Zaid Bin Mahbub, et al. 2020. Reliable tuberculosis detection using chest x-ray with deep learning, segmentation and visualization. *Ieee Access*, 8:191586–191601.
- MOHD ZAID RASHID. 2024. Oral cancer dataset. <https://www.kaggle.com/datasets/zaidpy/oral-cancer-dataset>. Kaggle.
- Sucheng Ren, Xiaoke Huang, Xianhang Li, Junfei Xiao, Jieru Mei, Zeyu Wang, Alan Yuille, and Yuyin Zhou. 2024. Medical vision generalist: Unifying medical imaging tasks in context. *arXiv preprint arXiv:2406.05565*.
- Manuel Alejandro Rodríguez, Hasan AlMarzouqi, and Panos Liatsis. 2022. Multi-label retinal disease classification using transformers. *IEEE Journal of Biomedical and Health Informatics*.
- Veronica Rotemberg, Nicholas Kurtansky, Brigid Betz-Stablein, Liam Caffery, Emmanouil Chousakos, Noel Codella, Marc Combalia, Stephen Dusza, Pascale Guitera, David Gutman, et al. 2021. A patient-centric dataset of images and metadata for identifying melanomas using clinical context. *Scientific data*, 8(1):34.
- Khaled Saab, Tao Tu, Wei-Hung Weng, Ryutaro Tanno, David Stutz, Ellery Wulczyn, Fan Zhang, Tim Strother, Chunjong Park, Elahe Vedadi, et al. 2024. Capabilities of gemini models in medicine. *arXiv preprint arXiv:2404.18416*.
- Salman Sajid. 2024. Oral diseases. <https://www.kaggle.com/datasets/salmansajid05/oral-diseases/data>. Kaggle.
- F Shaker. 2018. Human sperm head morphology dataset (hushem). *Mendeley Data*, 3.
- Julio Silva-Rodríguez, Adrián Colomer, María A Sales, Rafael Molina, and Valery Naranjo. 2020. Going deeper through the gleason scoring scale: An automatic end-to-end system for histology prostate grading and cribriform pattern detection. *Computer Methods and Programs in Biomedicine*, 195:105637.
- Eduardo Soares, Plamen Angelov, Sarah Biaso, Michele Higa Froes, and Daniel Kanda Abe. 2020. Sars-cov-2 ct-scan dataset:a large dataset of real patients ct scans for sars-cov-2 identification. *Cold Spring Harbor Laboratory Press*.
- Malliga Subramanian, Kogilavani Shanmugavadivel, Obuli Sai Naren, K Premkumar, and K Rankish. 2022. Classification of retinal oct images using deep learning. In *2022 International Conference on Computer Communication and Informatics (ICCCI)*, pages 1–7.
- Summers and Ronald. 2020. Chestxray nihcc. <https://nihcc.app.box.com/v/ChestXray-NIHCC/folder/36938765345>. NIH.
- SunneYi. 2021. Chest CT-Scan images Dataset.
- Siham Tabik, Anabel Gómez-Ríos, José Luis Martín-Rodríguez, Iván Sevillano-García, Manuel Rey-Area, David Charte, Emilio Guirado, Juan-Luis Suárez, Julián Luengo, MA Valero-González, et al. 2020. Covidgr dataset and covid-sdnet methodology for predicting covid-19 based on chest x-ray images. *IEEE journal of biomedical and health informatics*, 24(12):3595–3605.
- Tao Tu, Shekoofeh Azizi, Danny Driess, Mike Schaekermann, Mohamed Amin, Pi-Chuan Chang, Andrew Carroll, Charles Lau, Ryutaro Tanno, Ira Ktena, et al. 2024. Towards generalist biomedical ai. *NEJM AI*, 1(3):A10a2300138.

- Peking University. 2019. Odir-2019 dataset. <https://odir2019.grand-challenge.org/introduction/>. Grand Challenge.
- Preet Viradiya. 2020. Brain tumor dataset. <https://www.kaggle.com/datasets/preetviradiya/brain-tumor-dataset>. Kaggle.
- Haiyang Wang, Hao Tang, Li Jiang, Shaoshuai Shi, Muhammad Ferjad Naeem, Hongsheng Li, Bernt Schiele, and Liwei Wang. 2025. Git: Towards generalist vision transformer through universal language interface. In *European Conference on Computer Vision*, pages 55–73. Springer.
- Linda Wang, Zhong Qiu Lin, and Alexander Wong. 2020. Covid-net: a tailored deep convolutional neural network design for detection of covid-19 cases from chest x-ray images. *Scientific Reports*, 10(1):19549.
- Peng Wang, Shuai Bai, Sinan Tan, Shijie Wang, Zhihao Fan, Jinze Bai, Keqin Chen, Xuejing Liu, Jialin Wang, Wenbin Ge, Yang Fan, Kai Dang, Mengfei Du, Xuancheng Ren, Rui Men, Dayiheng Liu, Chang Zhou, Jingren Zhou, and Junyang Lin. 2024a. Qwen2-vl: Enhancing vision-language model’s perception of the world at any resolution. *arXiv preprint arXiv:2409.12191*.
- Peng Wang, Shuai Bai, Sinan Tan, Shijie Wang, Zhihao Fan, Jinze Bai, Keqin Chen, Xuejing Liu, Jialin Wang, Wenbin Ge, Yang Fan, Kai Dang, Mengfei Du, Xuancheng Ren, Rui Men, Dayiheng Liu, Chang Zhou, Jingren Zhou, and Junyang Lin. 2024b. Qwen2-vl: Enhancing vision-language model’s perception of the world at any resolution. *Preprint*, arXiv:2409.12191.
- Wenhai Wang, Zhe Chen, Xiaokang Chen, Jiannan Wu, Xizhou Zhu, Gang Zeng, Ping Luo, Tong Lu, Jie Zhou, Yu Qiao, et al. 2024c. Visionllm: Large language model is also an open-ended decoder for vision-centric tasks. *Advances in Neural Information Processing Systems*, 36.
- Xiaosong Wang, Yifan Peng, Le Lu, Zhiyong Lu, Mohammadhadi Bagheri, and Ronald M Summers. 2017. Chestx-ray8: Hospital-scale chest x-ray database and benchmarks on weakly-supervised classification and localization of common thorax diseases. In *Proceedings of the IEEE conference on computer vision and pattern recognition*, pages 2097–2106.
- wjXiaochuangw. 2019. [Covid-19-ct scan images](#).
- Zhenlin Xu, Marc Niethammer, and Colin A Raffel. 2022. Compositional generalization in unsupervised compositional representation learning: A study on disentanglement and emergent language. *Advances in Neural Information Processing Systems*, 35:25074–25087.
- Anna Zawacki, Carol Wu, George Shih, Julia Elliott, Mikhail Fomitchev, Mohannad Husain, Paras Lakhani, Phil Culliton, and Shunxing Bao. 2019. Siim-acr pneumothorax segmentation. <https://kaggle.com/competitions/siim-acr-pneumothorax-segmentation>. Kaggle.
- Yaya Zha. 2021. Rus-chn. <https://aistudio.baidu.com/datasetdetail/69582/0>. AI Studio.
- Ao Zhang, Liming Zhao, Chen-Wei Xie, Yun Zheng, Wei Ji, and Tat-Seng Chua. 2023a. Next-chat: An lmm for chat, detection and segmentation. *arXiv preprint arXiv:2311.04498*.
- Edward Zhang and Sauman Das. 2022. Glaucoma detection. <https://www.kaggle.com/datasets/sshikamaru/glaucoma-detection>. Kaggle.
- Ruipeng Zhang, Qinwei Xu, Chaoqin Huang, Ya Zhang, and Yanfeng Wang. 2022. Semi-supervised domain generalization for medical image analysis. In *2022 IEEE 19th International Symposium on Biomedical Imaging (ISBI)*, pages 1–5. IEEE.
- Shilong Zhang, Peize Sun, Shoufa Chen, Min Xiao, Wenqi Shao, Wenwei Zhang, Yu Liu, Kai Chen, and Ping Luo. 2023b. Gpt4roi: Instruction tuning large language model on region-of-interest. *arXiv preprint arXiv:2307.03601*.
- Tao Zhang, Xiangtai Li, Hao Fei, Haobo Yuan, Shengqiong Wu, Shunping Ji, Change Loy Chen, and Shuicheng Yan. 2024a. Omg-llava: Bridging image-level, object-level, pixel-level reasoning and understanding. In *NeurIPS*.
- Xiaoman Zhang, Chaoyi Wu, Ziheng Zhao, Weixiong Lin, Ya Zhang, Yanfeng Wang, and Weidi Xie. 2023c. Pmc-vqa: Visual instruction tuning for medical visual question answering. *arXiv preprint arXiv:2305.10415*.
- Yuhui Zhang, Alyssa Unell, Xiaohan Wang, Dhruva Ghosh, Yuchang Su, Ludwig Schmidt, and Serena Yeung-Levy. 2024b. Why are visually-grounded language models bad at image classification? *arXiv preprint arXiv:2405.18415*.
- Jinyu Zhao, Yichen Zhang, Xuehai He, and Pengtao Xie. 2020. Covid-ct-dataset: a ct scan dataset about covid-19. *arXiv preprint arXiv:2003.13865*.
- Chuang Zhu, Wenkai Chen, Ting Peng, Ying Wang, and Mulan Jin. Hard sample aware noise robust learning for histopathology image classification. *IEEE transactions on medical imaging*.
- Chuang Zhu, Wenkai Chen, Ting Peng, Ying Wang, and Mulan Jin. 2021. Hard sample aware noise robust learning for histopathology image classification. *IEEE transactions on medical imaging*, 41(4):881–894.

Table 5: Result of NEXT-Chat on CG by using detection and classification tasks to generalize classification Target dataset. Generalization results on classification datasets: "Related Combination" is the training set, "Target Subset" is the goal. Baseline and Trained represent the model’s accuracy without training and trained on related data, respectively. Green section indicates successful generalization, while red section denotes failure. The 4 segmented areas represent different Direction Types: fixed modality, fixed area, and modality-area paired combinations.

Related Combination		Target Subset	Baseline	Trained
Lung, Lung Det	Bones, Diseases	Lung, Diseases	49	52
Lung, Lung Det	Breast, Diseases	Lung, Diseases	49	54
Bones, Spinal Error Det	Breast, Diseases	Bones, Diseases	20	30
Bones, Spinal Error Det	Lung, Diseases	Bones, Diseases	20	33
MRI, Diseases Det	End, Level	End, Diseases	24	27
X-ray, Lung Det	CT, COVID	X-ray, COVID	23	26
Der, Skin, Cancer Det	FP, Fundus, Diseases	Der, Skin, Diseases	24	29
Mic, Cell, Cancer Det	CT, Kidney, Diseases	Mic, Cell, Diseases	24	26

Table 6: Result of MiniGPT-v2 on CG by using detection and classification tasks to generalize classification Target dataset. Generalization results on classification datasets: "Related Combination" is the training set, "Target Subset" is the goal. Baseline and Trained represent the model’s accuracy without training and trained on related data, respectively. Green section indicates successful generalization, while red section denotes failure. The 3 segmented areas represent different Direction Types: fixed modality, fixed area, and modality-area paired combinations.

Related Combination		Target Subset	Baseline	Trained
Lung, Lung Det	Bones, Diseases	Lung, Diseases	41	47
Lung, Lung Det	Breast, Diseases	Lung, Diseases	41	49
Bones, Spinal Error Det	Breast, Diseases	Bones, Diseases	31	35
Bones, Spinal Error Det	Lung, Diseases	Bones, Diseases	31	37
MRI, Diseases Det	End, Level	End, Diseases	24	26
X-ray, Lung Det	CT, COVID	X-ray, COVID	22	23
Der, Skin, Cancer Det	FP, Fundus, Diseases	Der, Skin, Diseases	27	30
Mic, Cell, Cancer Det	CT, Kidney, Diseases	Mic, Cell, Diseases	20	24

Table 7: Result of Qwen2-VL on selected classification datasets in Med-MAT. Green section indicates successful generalization, while red section denotes failure.

Related Combination		Target Subset	Baseline	Trained
Bones, State	Breast, Diseases	Bones, Diseases	61	65
Lung, COVID	Bones, Diseases	Lung, Diseases	80	91
CT, COVID	X-ray, Diseases	X-ray, COVID	35	40
CT, State	X-ray, Diseases	X-ray, State	35	43
X-ray, Lung	CT, Brain(Cancer)	CT, Lung	32	33
X-ray, Lung	CT, Brain	CT, Lung(Cancer)	65	72
FP, Fundus, Diseases	Mic, Cell, Level	FP, Fundus, Level	48	45
Mic, Cell, Cell Identification	FP, Fundus, Level	Mic, Cell, Level	34	41

source specification will be provided in B.3.

B.1 Details of MAT-Triplet

MAT-Triplet stands for Medical Modality, Anatomical Area, and Medical Task. We define all samples in Med-MAT using these three components and integrate datasets with identical triplets into subsets.

Medical Modality refers to different types of

techniques or methods used in medical imaging or data acquisition. Each modality is designed to present the human body’s structures or pathological features in unique ways, providing auxiliary support for clinical diagnosis and treatment. Most modalities exhibit significant visual differences, making them easily distinguishable. Med-MAT encompasses 11 modalities, including common ones such as Computed Tomography (CT), Magnetic

Table 8: Result of Llama-3.2-Vision on selected classification datasets in Med-MAT. Green section indicates successful generalization, while red section denotes failure.

Related Combination		Target Subset	Baseline Trained	
Bones, State	Breast, Diseases	Bones, Diseases	52	59
Lung, COVID	Bones, Diseases	Lung, Diseases	64	75
CT, COVID	X-ray, Diseases	X-ray, COVID	33	38
CT, State	X-ray, Diseases	X-ray, State	33	41
X-ray, Lung	CT, Brain(Cancer)	CT, Lung	31	29
X-ray, Lung	CT, Brain	CT, Lung(Cancer)	49	57
FP, Fundus, Diseases	Mic, Cell, Level	FP, Fundus, Level	55	61
Mic, Cell, Cell Identification	FP, Fundus, Level	Mic, Cell, Level	10	32

Resonance Imaging (MRI), X-ray, Fundus Photography (FP), Endoscopy (End), Optical Coherence Tomography (OCT), and Ultrasound (US), as well as rare and specialized modalities like Colonoscopy (Co), Dermoscopy (Der), Digital Pathology (DP), and Microscopy (Mic).

Anatomical Area refers to specific anatomical structures or regions within the human body or other organisms, defined by distinct anatomical characteristics to describe various body parts, their functions, and relative positions. Med-MAT encompasses 14 anatomical areas, including the cervix, kidney, lung, brain, intestine, bladder, fundus, retina, breast, bones, and chest. To further facilitate data description, additional categories such as skin, mouth, and cell are included as specialized anatomical areas.

Medical Task refers to the specific detection task that needs to be performed on the dataset. Med-MAT includes 13 distinct tasks, with classification tasks encompassing Quality Identification (image quality analysis), COVID Diagnosis, Cancer Diagnosis (determining the presence of a specific disease), State (such as identifying brain hemorrhage), Level Identification (assessing disease severity), and Multiple Classification (classifying multiple diseases or cell types). Given the limited options of COVID Diagnosis and Cancer Diagnosis, these tasks can be interpreted as identifying whether a patient is in a diseased state. To enhance generalization and provide more diverse examples, these tasks are grouped under the broader category of State. In addition, we have 16 datasets defining segmentation or classification tasks with different objectives.

B.2 QA construction method

A large amount of image-label datasets was collected to build the Med-MAT dataset. To ensure compatibility with MLLM training inputs and

outputs, all data is transformed into a question-answering format. Questions are formulated based on modality, anatomical area, and medical task, with 6 question prompts applied to each subset.

The labels within each data subset will be clustered to prevent redundant definitions of the same condition. Then, all training set and test set will be converted into multiple-choice questions following the template in Table 8. Each question will have up to four options, with distractor options randomly selected from the corresponding subset.

B.3 Data composition and Open-source Specification

Med-MAT is composed of multiple datasets. After being transformed into different QA formats, the new data is organized into several subsets to support generalization experiments in medical imaging. Table 9 shows all of our subset datasets, which are separated based on different combinations in MAT-Triplet. The specific MAT-Triplets are listed, along with the labels corresponding to the image-label datasets for each subset. Correspondingly, all the image-label datasets are also displayed in Table 10, which includes their names, descriptions of the tasks performed, download links, and the level of accessibility.

All question-answering text datasets in Med-MAT will be publicly available. To accommodate varying access permissions, we will release datasets based on their respective licenses: openly accessible datasets will be directly available, while restricted datasets can be accessed by applying through the links provided in this paper. We hope this dataset will support and advance future generalization experiments on medical imaging.

Multiple-choice Questions Template

<question>

A. <option_1>

B. <option_2>

C. <option_3>

D. <option_4>

Answer with the option's letter from the given choices directly.

Figure 8: The Template of multiple-choice questions.

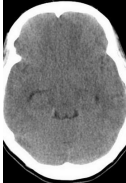
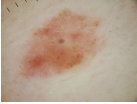

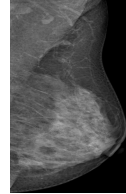


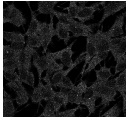

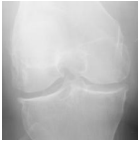
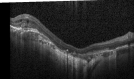
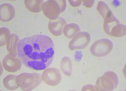
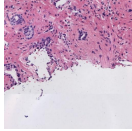
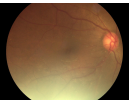
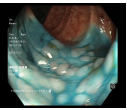

 <p>Q: Assess this brain CT image and reply 'Hemorrhage' if visible, or 'Normal' if no hemorrhage is present.</p> <p>A. Hemorrhage B. Normal</p>	 <p>Q: Please examine this dermoscopic image and identify the condition present.</p> <p>A. Benign skin lesion B. Nevus C. Malignant dermal D. Genodermatoses</p>	 <p>Q: Please examine this bladder image taken during endoscopy and determine the type of cancer present.</p> <p>A. No tumor lesion B. Low-grade carcinoma C. High-grade carcinoma D. Non-suspicious tissue</p>
 <p>Q: You are viewing a mammogram. Kindly assess the conditions shown in the image, separating multiple conditions with commas. If no condition is present, return 'Normal'.</p> <p>A. Normal B. Asymmetry C. Nipple retraction D. Mass</p>	 <p>Q: This is a spine X-ray image. Kindly assess the type of spinal pathology.</p> <p>A. Surgical implant B. Foraminal stenosis C. Other lesions D. Osteophytes</p>	 <p>Q: Shown here is an X-ray of a bone. Please determine the appropriate age category.</p> <p>A. 7 B. 6 C. 9 D. 11</p>
 <p>Q: This image contains human protein cells. Please list their types, separating each one with a comma.</p> <p>A. Centrosome, cytosol B. Centrosome, nucleoplasm C. Intermediate filaments D. Cytosol</p>	 <p>Q: Review this chest X-ray image and specify the type of pneumonia if found, or return 'Normal' if no condition is present.</p> <p>A. Secondary ptb B. Covid C. Left ptb D. Right upper ptb</p>	 <p>Q: Please examine this X-ray image of a bone and rate the severity of arthritis from 0 to 4.</p> <p>A. Level 1 B. Level 2 C. Level 3 D. Level 0</p>
 <p>Q: This is an OCT image. Please identify any condition present.</p> <p>A. Drusen B. Choroidal neovascularization C. Normal D. Age-related macular degeneration</p>	 <p>Q: This is an image of cells taken under a microscope. Please identify all the cells present (separate multiple cell types with a comma).</p> <p>A. Eosinophil, lymphocyte B. Neutrophil, eosinophil C. Lymphocyte, lymphocyte D. Neutrophil</p>	 <p>Q: Please examine this microscopic image and determine the cancer grade of the prostate.</p> <p>A. Gg3 B. No cancer C. Gg4 D. Gg5</p>
 <p>Q: Please assess this fundus image and list all conditions present, using commas to separate them. If no conditions are detected, return 'Normal'.</p> <p>A. Mild nonproliferative retinopathy B. Central serous retinopathy C. Choriorretinal atrophy, epiretinal membrane D. Media haze, optic disc pallor</p>	 <p>Q: Review this image from the endoscopy and specify any intestinal diseases detected.</p> <p>A. Polyps B. Normal cecum C. Dyed lifted polyps D. Dyed resection margins</p>	 <p>Q: This is an image taken during an endoscopy. Please assess the cleanliness level of the intestine, rating it from 0 to 3.</p> <p>A. 3 B. 1 C. 2 D. 0</p>

Figure 9: Illustration of diverse samples with varying numbers of candidate options in the Med-MAT dataset.

Table 9: The details of subset. In particular, **Co** stands for Colposcopy, **CT** represents Computed Tomography, **DP** refers to Digital Photography, **FP** is for Fundus Photography, **MRI** denotes Magnetic Resonance Imaging, **OCT** signifies Optical Coherence Tomography, **Der** refers to Dermoscopy, **End** stands for Endoscopy, **Mic** indicates Microscopy Images, and **US** represents Ultrasound. The blue section represents the classification dataset and the green section represents the detection

Subset No.	Modality	Anatomical Area	Task	Datasets No.
01	Co	Cervix	Cervical Picture Quality Evaluation	1
02	CT	Kidney	Kidney Diseases Classification	2
03	CT	Lung	COVID-19 Classification	3,4,6
04	CT	Lung	Lung Cancer Classification	5
05	CT	Brain	Brain Hemorrhage Classification	7
06	CT	Brain	Brain Cancer Classification	8
07	Der	Skin	Melanoma Type Classification	10
08	Der	Skin	Skin Diseases Classification	9, 11-15, 71, 72, 74
09	DP	Mouth	Teeth Condition Classification	16
10	DP	Mouth	Oral Cancer Classification	17
11	End	Intestine	Intestine Cleanliness Level	18
12	End	Bladder	Cancer Degree Classification	19
13	End	Intestine	Intestine Diseases Classification	20
14	FP	Fundus	Eye Diseases Classification	21-23, 26-28, 31, 32, 75
15	FP	Fundus	Multiple-labels Eye Diseases Classification	24, 25, 68
16	FP	Fundus	Blindness Level	29
17	FP	Fundus	Retinal Images Quality Evaluation	30
18	Mic	Cell	Cell Type Classification	33, 36-38, 39-41, 44, 65, 70
19	Mic	Cell	Prostate Cancer Degree Classification	34
20	Mic	Cell	Multiple-labels Blood Cell Classification	35
21	Mic	Cell	Cancer Classification	42, 67
22	MRI	Brain	Head Diseases Classification	44, 45
23	OCT	Retina	Retina Diseases Classification	46, 47
24	US	Breast	Breast Cancer Classification	48
25	X-ray	Bones	Degree Classification of Knee	49, 53
26	X-ray	Bones	Fractured Classification	50, 51
27	X-ray	Bones	Vertebrae Diseases Classification	52
28	X-ray	Lung	COVID-19 and Pneumonia Classification	54-57, 60, 62, 81
29	X-ray	Breast	Breast Diseases Classification	58, 78
30	X-ray	Lung	Tuberculosis Classification	59, 79
31	X-ray	Chest	Multiple-labels Chest Classification	61, 73, 76, 77, 80, 85, 87
32	X-ray	Brain	Tumor Classification	63
33	Mic	Cell	Multi-labels Diseases	84
34	FP	Fundus	Level Identification	66
35	X-ray	Bones	Level Identification	69
36	X-ray	Bones	Spinal lesion Classification	86
37	X-ray	Breast	Multi-labels Diseases	82
38	Der	Skin	Lesion Det/Seg	88-91
39	End	Intestine	PolyP Det/Seg	92-93
40	End	Intestine	Surgical Procedures Det/Seg	94
41	End	Intestine	Multi-labels Det/Seg	95
42	Mic	Cell	Cancer Cell Det/Seg	96
43	US	Chest	Cancer Det/Seg	97
44	US	Thyroid	Thyroid Nodule Region Det/Seg	98
45	MRI	Intestine	Multi-labels Det/Seg	103
46	MRI	Liver	Liver Det/Seg	104, 105
47	X-ray	Lung	Lung Det/Seg	99
48	X-ray	Lung	Pneumothorax Det/Seg	106
49	X-ray	Bones	Spinal Anomaly Det	100
50	X-ray	Chest	Multi-labels Det	101, 102
51	FP	Fundus	Vessel Seg	107
52	FP	Fundus	Optic Disc and Cup Seg	108
53	FP	Fundus	Optic Disc Seg	109

Table 10: The details of the medical datasets are provided

No.	Name	Description	Citation
1	Intel & MobileODT Cervical Screening	Cervix Type in Screening	(BenO et al., 2017)
2	CT Kindney Dataset	Normal or Cyst or Tumor	(Islam et al., 2022a)
3	SARS-COV-2 Ct-Scan	COVID19, Classification Dataset	(Soares et al., 2020)
4	COVID CT COVID-CT	COVID19, Classification Dataset.	(Zhao et al., 2020)
5	Chest CT-Scan	Cancer Classification	(SunneYi, 2021)
6	COVID-19-CT SCAN IMAGES	COVID19, Classification	(wjXiaochuangw, 2019)
7	Head CT	Head Hemorrhage	(Kitamura, 2018)
8	CT of Brain	Head Cancer	(Data, 2023)
9	MED-NODE	Melanoma or Naevus	(Giotis et al., 2015)
10	ISIC 2020	Melanoma, Benign or Malignant	(Rotemberg et al., 2021)
11	PED-UFES-20	Skin Multi Classification	(Pacheco et al., 2020)
12	Web-scraped Skin Image	Skin Disease Multi Classification	(Islam et al., 2022b)
13	ISBI 2016	Skin Lesion Classification	(Gutman et al., 2016)
14	ISIC 2019	Skin Disease Multi Classification	(Combalia et al., 2019)
15	Skin Cancer ISIC	Skin Cancer Multi Classification	(Katanskiy, 2019)
16	Dental Condition Dataset	Teeth condition classification	(Sajid, 2024)
17	Oral Cancer Dataset	Oral cancer Classification	(RASHID, 2024)
18	The Nerthus Dataset	Cleanliness level	(Pogorelov et al., 2017a)
19	Endoscopic Bladder Tissue	Canser Degree Classification	(Lazo et al., 2023)
20	Kvasir	Multi Disease Classification	(Pogorelov et al., 2017b)
21	ACRIMA	Glaucoma	(Ovreiu et al., 2021)
22	Augemnted ocular diseases AOD	Multi Classification of eye diseases	(Б а т ы б е к л ы , 2021)
23	JSIEC	Multi Classification of eye diseases	(Cen et al., 2021)
24	Multi-Label Retinal Diseases	Multi Classification of eye diseases	(Rodríguez et al., 2022)
25	RFMiD 2.0	Multi Classification of eye diseases	(Panchal et al., 2023)
26	ToxoFundus(Data Processed Paper)	Ocular toxoplasmosis	(Cardozo et al., 2023)
27	ToxoFundus(Data Raw 6class All)	Ocular toxoplasmosis	(Cardozo et al., 2023)
28	Adam dataset	Age-related Macular Degeneration	(Liang, 2021)
29	APTOS 2019 Blindness	Blindness Level Identification 0 4	(Karthik et al., 2019)
30	DRIMBD	Quality Testing of Retinal Images	(Prentasic et al., 2013)
31	Glaucoma Detection	Glaucoma Classification	(Zhang and Das, 2022)
32	AIROGS	Glaucoma Classification	(de Vente et al., 2023)
33	ICPR-HEp-2	Multi Classification	(Qi et al., 2016)
34	SICAPv2	Cancer Degree Classification	(Silva-Rodríguez et al., 2020)
35	Blood Cell Images	Blood Cell Classificaion (Multi)	(Mooney, 2017)
36	BreakHis	Cell type and beginormag	(Bukun, 2019)
37	Chaoyang	Multi Classification of pathologists	(Zhu et al.)
38	HuSHeM	Sperm Head Morphology Classificaion	(Shaker, 2018)
39	Bone Marrow Cell Classification	Bone Marrow Cell Classification	(Matek et al., 2021)
40	NCT-CRC-HE-100K	Multi Classification	(Kather et al., 2018)
41	Malignant Lymphoma Classification	Multi Classification	(Orlov et al., 2010a)
42	Histopathologic Cancer Detection	Cancer Classification	(Cukierski, 2018)
43	LC25000	Multi Classification of Lung and Colon	(Zhu, 2022)
44	Brain Tumor 17 Classes	Multi Classification	(Feltrin, 2022)
45	Tumor Classification	Pituitary or Glioma or Meningioma or Notumor	(Nickparvar, 2021a)
46	Malignant Lymphoma Classification	Multi Classification of eye diseases	(Orlov et al., 2010b)
47	Retinal OCT-C8	Multi Classification of eye diseases	(Subramanian et al., 2022)
48	BUSI	Breast Cancer	(Al-Dhabyani et al., 2020)
49	Digital Knee X-Ray Images	Degree Classification of Knee	(Gornale and Patravali, 2020)
50	Bone Fracture Multi-Region X-ray Data	Fractured Classification	(Nickparvar, 2021b)
51	Fracture detection	Fractured Classification	(Batra, 2024)
52	The vertebrae X-ray image	Vertebrae	(Fraiwan et al., 2022)
53	Knee Osteoarthritis Dataset	Knee Osteoarthritis with severity grading	(Chen, 2018)
54	Shenzhen Chest X-Ray Set	COVID19, Classification Dataset.	(Jaeger et al., 2014)
55	Chest X-ray PD	COVID and Pneumonia	(Asraf and Islam, 2021)
56	COVID-19 CHEST X-RAY DATABASE	COVID and Pneumonia	(Chowdhury et al., 2020)
57	COVIDGR	COVID19, Classification	(Tabik et al., 2020)
58	MIAS	Multi Classification of Breast	(Mader, 2017)
59	Tuberculosis Chest X-Ray Database	Tuberculosis	(Rahman et al., 2020)
60	Pediatric Pneumonia Chest X-Ray	Pneumonia Classification	(Kermany, 2018)

Table 11: Continued from Table 10.

No.	Name	Description	Citation
61	Random Sample of NIH Chest X-Ray Dataset	Multi Classification of Chest	(Wang et al., 2017)
62	CoronaHack-Chest X-Ray	Pneumonia Classification with Virus type	(Praveen, 2019)
63	Brain Tumor Dataset	Tumor Classification	(Viradiya, 2020)
64	Fitzpatrick 17k (Nine Labels)	Multi Classification	(Groh et al., 2021)
65	BioMediTech	Multi Classification	(Nanni et al., 2016)
66	Diabetic retinopathy	Diabetic Retinopathy Level	(Benítez et al., 2021)
67	Leukemia	Cancer Classification	(Codella et al., 2019)
68	ODIR-5K	Multiple Labels Classification	(University, 2019)
69	Arthrosis	Bone Age Classification	(Zha, 2021)
70	HSA-NRL	Multi Classification of pathologists	(Zhu et al., 2021)
71	ISIC 2018 (Task 3)	Multi Classification	(Codella et al., 2019)
72	ISIC 2017 (Task 3)	Multi Classification	(Codella et al., 2018)
73	ChestX-Det	Multi Classification	(Lian et al., 2021)
74	Monkeypox Skin Lesion Dataset	Only Monkeypox	(Ali et al., 2022)
75	Cataract Dataset	Multi Classification	(JR2NGB, 2019)
76	ChestX-rays IndianaUniversity	Multi-label Classification	(Raddar, 2019)
77	CheXpert v1.0 small	Multi-label Classification	(Arevalo, 2020)
78	CBIS-DDSM	Multi Classification	(Lee et al., 2017)
79	NLM-TB	Tuberculosis	(Karaca, 2022)
80	ChestXray-NIHCC	Multi-label Classification	(Summers and Ronald, 2020)
81	COVIDx CXR-4	COVID19, Classification	(Wang et al., 2020)
82	VinDr-Mammo	Multi-label Classification	(Nguyen et al., 2023)
83	PBC dataset normal DIB	Multi Classification	(Acevedo et al., 2020)
84	Human Protein Atlas	Multi-label Classification (Only green)	(Le et al., 2022)
85	RSNA Pneumonia Detection Challenge 2018	Multi-label Classification	(Anouk Stein et al., 2018)
86	VinDr-SpineXR	Multi Classification of Bones Diseases	(Pham et al., 2021)
87	VinDr-PCXR	Multi-label Classification	(Pham et al., 2022)
88	PH2	Melanoma Segmentation	(Mendonca et al., 2015)
89	ISBI 2016 (Task3B)	Melanoma Segmentation	(Gutman et al., 2016)
90	ISIC 2016 (Task 1)	Melanoma Segmentation	(Gutman et al., 2016)
91	ISIC 2017	Melanoma Segmentation	(Codella et al., 2018)
92	CVC-ClinicDB	Polyp Segmentation	(Bernal et al., 2015)
93	Kvasir-SEG	Polyp segmentation	(Jha et al., 2020)
94	m2caiseg	Surgical Instrument Segmentation	(Maqbool et al., 2020)
95	EDD 2020	Multiple Diseases Segmentation in Intestine	(Ali et al., 2020)
96	SICAPv2	Cancer Cells Segmentation	(Silva-Rodríguez et al., 2020)
97	BUSI	Cancer Segmentation	(Hesaraki, 2022)
98	TN3K	Thyroid Nodule Segmentation	(Gong et al., 2022)
99	NLM-TB	Lung Segmentation (With left or right)	(Gong et al., 2021)
100	VinDr-SpineXR	Spinal X-ray Anomaly Detection	(Pham et al., 2021)
101	VinDr-PCXR	Multiple Diseases Segmentation in Chest	(Pham et al., 2022)
102	ChestX-Det	Multiple Diseases Segmentation in Chest	(Lian et al., 2021)
103	UW-Madison GI Tract Image Segmentation	Surgical Instrument Segmentation	(Lee et al., 2024)
104	Duke Liver Dataset MRI v1	Liver Segmentation	(Macdonald et al., 2020)
105	Duke Liver Dataset MRI v2	Liver Segmentation	(Macdonald et al., 2020)
106	SIIM-ACR Pneumothorax Segmentation	Pneumothorax Segmentation	(Zawacki et al., 2019)
107	FIVES	Fundus Vascular Segmentation	(Jin et al., 2022)
108	RIM-ONE DL	Optic Disc and Cup Segmentation	(Batista et al., 2020)
109	PALM19	Optic Disc Segmentation	(Fu et al., 2019)